Sex and Laterality Differences in Medullary Humerus Morphology

ALEX J. DREW,[2,3] ROBERT Z. TASHJIAN,[1,2] HEATH B. HENNINGER,[2,3] AND KENT N. BACHUS [1,2,3]*

[1]Rehabilitation Research and Development Service, VA Medical Center, Salt Lake City, Utah
[2]Department of Orthopaedics, University of Utah, Salt Lake City, Utah
[3]Department of Biomedical Engineering, University of Utah, Salt Lake City, Utah

ABSTRACT

Percutaneous osseointegrated (OI) prosthetic limb attachment holds promise for transhumeral amputees. Understanding humeral medullary morphology is necessary for informed design of upper extremity OI systems, and is beneficial to the field of megaprosthetic reconstruction of the distal humerus where diaphyseal fixation is desired. The purpose of this study was to quantify the sex and laterality differences in humerus morphology, specifically over the diaphysis. Three-dimensional surface reconstructions of 58 pairs of cadaveric humeri (43 male, 15 female) were generated from CT data. Measures describing periosteal and medullary morphology were collected relative to an anatomic coordinate system. Sex and laterality differences in biomechanical length (BML) were observed ($P \leq 0.001$ and 0.022, respectively). Head radius was larger in males than females ($P \leq 0.001$). Retroversion was increased in right humeri relative to left ($P \leq 0.001$). Canal orientation exhibited a conformational shift from anteversion to retroversion distally at approximately 65% BML. Right humeri exhibited larger medullary diameters than left in the 1st and 2nd principal directions ($P \leq 0.024$). Males displayed larger diameter medullary canals proximally ($P \leq 0.029$) and an increased rate of divergence of the endosteal cortex in the proximal diaphysis ($P \leq 0.009$). Females exhibited higher canal aspect ratios at mid-shaft ($P \leq 0.014$) and lower mean cortical thickness ($P \leq 0.001$). Human humeral diaphysis morphology exhibits sex and laterality differences, which are dependent on position along the diaphysis. Understanding humeral morphology is necessary to achieve adequate primary stability and bone apposition in design of endoprosthetic stems for percutaneous OI implants, and distal humerus replacement. Anat Rec, 302:1709–1717, 2019. © 2019 The Authors. *The Anatomical Record* published by Wiley Periodicals, Inc. on behalf of American Association for Anatomy

Key words: humerus; morphology; medullary canal; periosteum; sex; laterality

Socket suspensions that fit over the residual limb of an amputee represent the standard of care in prosthetic limb attachment. Unfortunately, socket suspensions do not meet the needs of many upper extremity amputees, resulting in up to 39% of above elbow amputees rejecting use of a prosthetic (Biddiss and Chau, 2007a, 2007b). Negative factors

Grant sponsor: United States Department of Veterans Affairs Rehabilitation Research and Development Service; Grant number: I01RX001246; Grant sponsor: US Army Medical Research and Materiel Command; Grant number: W81XWH-15-C-0058.

*Correspondence to: Kent N. Bachus, Orthopaedic Research Laboratory, University of Utah Orthopaedic Center, 590 Wakara Way, Salt Lake City Utah 84108. Tel: 801.587.5206, Fax: 801.587.5211 E-mail: kent.bachus@hsc.utah.edu

Received 6 December 2018; Revised 6 February 2019; Accepted 22 February 2019.

DOI: 10.1002/ar.24138
Published online 15 April 2019 in Wiley Online Library (wileyonlinelibrary.com).

related to socket suspensions, including discomfort, low functionality, lack of heat dissipation, and inconvenience, are primary drivers of device abandonment, and rank high in consumer design priorities (Biddiss et al., 2007; Biddiss and Chau, 2007a, 2007b; Berke et al., 2010). Recent advancement in the field of percutaneous osseointegrated (OI) prosthetic limb attachment have resulted in the emergence of cementless, press-fit, intramedullary stems for fixation of upper and lower extremity exoprostheses (Hagberg and Branemark, 2009; Kang et al., 2010; Jonsson et al., 2011; Juhnke et al., 2015; Al Muderis et al., 2016).

Percutaneous OI systems rely on adequate initial fixation, and circumferential fill of the medullary canal, for bone ingrowth and long-term stability (Engh et al., 1992; Shelton et al., 2011; Jeyapalina et al., 2014; Al Muderis et al., 2016). Additionally, such systems must be compatible with placement at multiple locations along the bone to accommodate variable amputation levels. Failure to satisfy these conditions may lead to premature implant loosening, and limit the clinical utility of the system. To facilitate successful design of these systems, a detailed description of the medullary diaphysis is necessary. To date, investigations of humeral morphology have largely been motivated by shoulder (Pearl and Volk, 1996; Robertson et al., 2000; Gebhart et al., 2013; Johnson et al., 2013) and elbow (Brownhill et al., 2007; Goldberg et al., 2007) arthroplasty, resulting in few investigations of diaphyseal medullary morphology (Descamps et al., 2009), but none examine the full length of the humeral diaphysis in detail.

The purpose of the present study was to utilize three-dimensional modeling techniques to investigate the medullary morphology of the humeral diaphysis, including medullary canal diameter, aspect ratio, taper, orientation, and cortical thickness, and relate these findings to the design of press-fit intramedullary stems for OI prosthetic attachment. Computed tomography (CT), three-dimensional modeling, and image processing techniques were employed for nondestructive analysis. We hypothesized that differences would arise between humeri based on gender and laterality of the bones.

MATERIALS AND METHODS

Fifty-eight pairs of fresh frozen cadaver humeri were obtained following a University of Utah Institutional Review Board exempt protocol (IRB #11755). The population contained 43 pairs from male donors with a median age of 51 years (range: 18–74 years), and 15 pairs from female donors with a median age of 53 years (21–66 years). Four donors were African American, one was Hispanic, and the remaining donors were Caucasian. Height, weight, and handedness information were not available. Soft tissue, if present, was removed by manual dissection. Humeral pairs with visual or radiographic skeletal abnormalities were excluded from the study.

CT Reconstruction and Accuracy Verification

Axial CT scans of all humeri were acquired using a Siemens SOMATOM Definition Flash scanner (120 kVp, 100 mAs, 512×512 acquisition matrix, 0.6-mm slice thickness, B50s kernel, 150-mm field-of-view). CT images were segmented and reconstructed in Amira (v5.4.1, FEI, Hillsboro, OR) using semi-automatic thresholding techniques to identify both the medullary (inner) and periosteal (outer) cortical surfaces. Three-dimensional surface reconstructions were generated from the respective segmentations. Interoperator surface reconstruction repeatability was assessed for three operators on a single humerus by comparison to reference periosteal and medullary surfaces generated by an experienced segmentation operator from high-resolution MicroCT (0.059-mm isotropic voxel spacing, PerkinElmer QuantumFX). Surface deviations from the MicroCT generated reference surface were calculated following iterative closest point alignment. Alignment and surface deviation analyses were performed in 3-Matic Research 18 (Materialise, Leuven, Belgium).

Anatomic Coordinate System

To align specimens and to provide a reference frame for morphologic measures, an anatomic coordinate system was defined. To increase applicability of the coordinate system definition to those with upper extremity amputation or trauma, only proximal humeral landmarks were employed in coordinate system calculation (Fig. 1A). The definition used here was adapted from the humeral coordinate system proposed by DeLude et al. (2007). The origin was established at the center of the humeral head using a sphere fit based on the convex articulating surface. The articulating surface was selected based on 1st principal curvature (PostView, www.febio.org) (Fig. 1B). Next the articulating margin plane (AMP) was established by further refining the selection of the convex region to isolate nodes at the transition from convex to concave at the anatomic neck and creating a best-fit plane (Fig. 1C). The normal vector to this AMP was the first vector needed for coordinate system generation. The second vector was a humeral shaft axis (HSA) calculated by fitting a line to the centroids of the medullary segmentation from mid-shaft (median slice) to one humeral head diameter below the origin (Fig. 1C). This range was selected to prevent lateral drift of the HSA due to the proximal metaphyseal flare. Using the AMP normal vector and HSA, the coordinate system was defined as follows (Figs. 1D,E):

- Origin: Coincident with the center of the sphere fit to the articulating surface of the humeral head.
- *Z*-axis: HSA, defined as a best-fit line through the centroid of the medullary canal from mid-shaft to one humeral head diameter below the origin.
- *X*-axis: Cross-product of AMP normal vector and Z. Positive in anterior direction.
- *Y*-axis: Cross-product of Z and X. Positive in medial direction.

Surface reconstructions of left humeri were mirrored prior to coordinate system generation to avoid the use of right- and left-handed coordinate systems.

External Morphology

Articulating (convex) surfaces of the trochlea and capitellum were also selected using 1st principal curvature. A best-fit cylindrical axis was calculated from these selections (Kapron et al., 2014). The cylindrical axis in conjunction with selections described for anatomic coordinate system generation were used to calculate biomechanical length (BML), humeral head radius (R), humeral head inclination (θ_I), and retroversion (θ_R) as follows (Fig. 2):

- BML: Distance along the *Z*-axis between the humeral head center and the mid-point of the distal cylindrical axis.

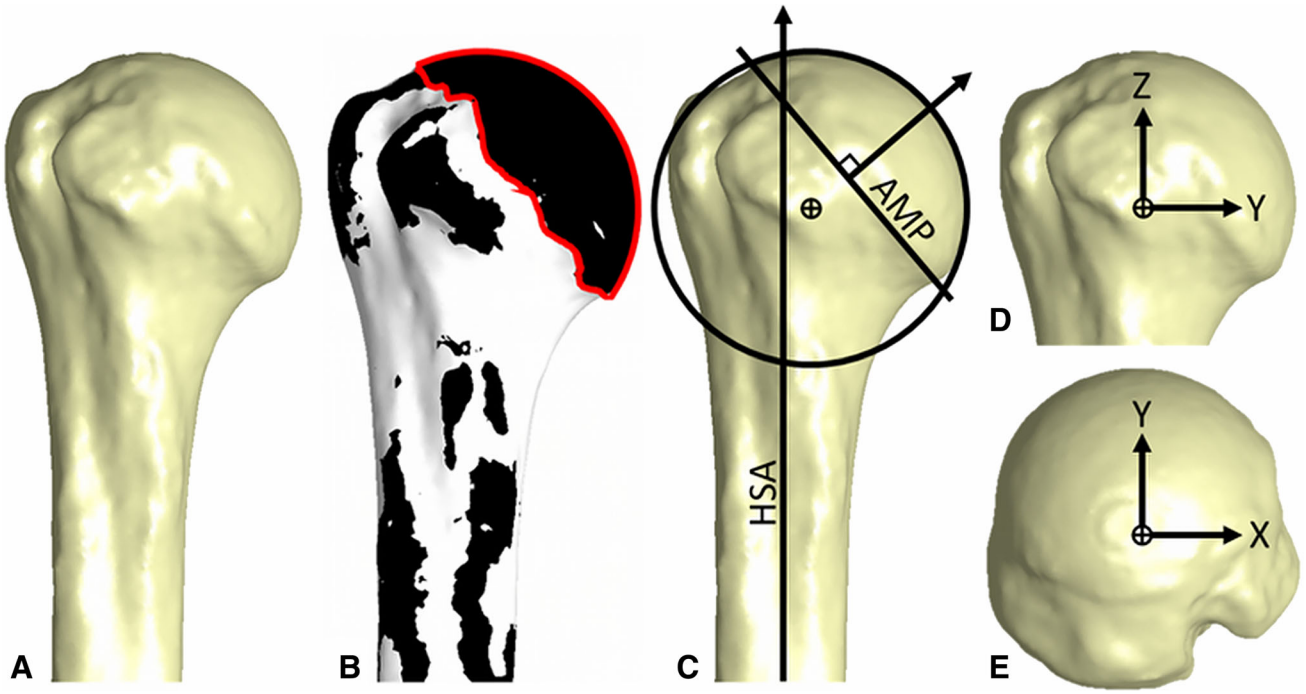

Fig. 1. (**A**) Anteroposterior (AP) view of a right proximal humerus. (**B**) Plot of 1st principal curvature with the convex surface (black) and articulating region (outlined in red). (**C**) Sphere fit of articulating region (circle), AMP, HSA. (**D**) AP view of the anatomic coordinate system. (**E**) Axial view of the anatomic coordinate system.

- R: Radius of sphere fit to articulating surface of the humeral head.
- θ_I: The angle between the *Z*-axis and the normal vector of the AMP.
- θ_R: The angle between the cylindrical axis and the *Y*-axis in the XY plane.

Medullary Morphology

Axial cross-sections of the aligned humeri were exported as binary images using Amira (ThermoFisher Scientific, Waltham, MA), with 0.1-mm resolution in the XY plane, at 1% increments of BML. Medullary cross-sections were subtracted from periosteal cross-sections yielding images containing only a continuous annulus of cortical bone (Fig. 3). A custom Matlab (Mathworks, Natick, MA) analysis script was used to calculate the following morphologic parameters from each binary axial cross-section:

- Medullary orientation: Angular orientation of the medullary canal with respect to the *Y*-axis. Orientation determined using principal component analysis (PCA).
- 1st principal diameter: Medullary diameter measured as the maximum projection of the medullary canal cross-section onto the medullary orientation axis.
- 2nd principal diameter: Medullary diameter orthogonal to the medullary orientation.
- Aspect ratio: 1st principal diameter/2nd principal diameter.
- Mean cortical thickness: Mean thickness of the cortical bone at each cross-section.

Distal and proximal cutoffs for diaphyseal analyses were established at 20% (proximal) and 80% (distal) of BML to exclude the metaphyseal flares.

Statistical Analyses

Interoperator repeatability for landmark selection and calculation of anatomic measures was assessed using the intraclass correlation coefficient (ICC). ICC estimates and their 95% confidence intervals were calculated based on a 2-way random-effects model for absolute agreement using 3 operators and 10 randomly selected humeri. ICC was calculated for each external morphologic measure. Paired t-tests were used to determine differences between right and left humeri with regard to head radius, inclination, retroversion, BML, and medullary measures at 20, 35, 50, 65, and 80% BML.

Independent t-tests were used to determine differences between male and female donors. To ensure that the unequal sample sizes between males and females would not have an outsized effect on statistical significance, bootstrapping was applied to all *P* values to establish the achieved significance level (ASL). Only trivial differences were observed between *P* values derived from the t-test and bootstrap ASL, confirming the robustness of the t-test for this analysis. In particular, no conclusion of significance was dependent on the choice of statistical test. Therefore, we report *P* values from the t-test, as these provide the most understandable presentation of the results and are consistent with other comparisons.

Taper of the medullary diameters in the 1st and 2nd principal directions were determined by piecewise linear regression for each group (right, left, male, female). This method yielded medullary expansion rates for the proximal and distal diaphysis as well as the inflection point at which the medullary taper changed as a function of length (Jones and Molitoris, 1984). A Wald test was then applied to the proximal, distal, and break point fit coefficients of the piecewise linear fit to determine differences between groups. Again, a bootstrapping approach was evaluated and no conclusion of significance was altered.

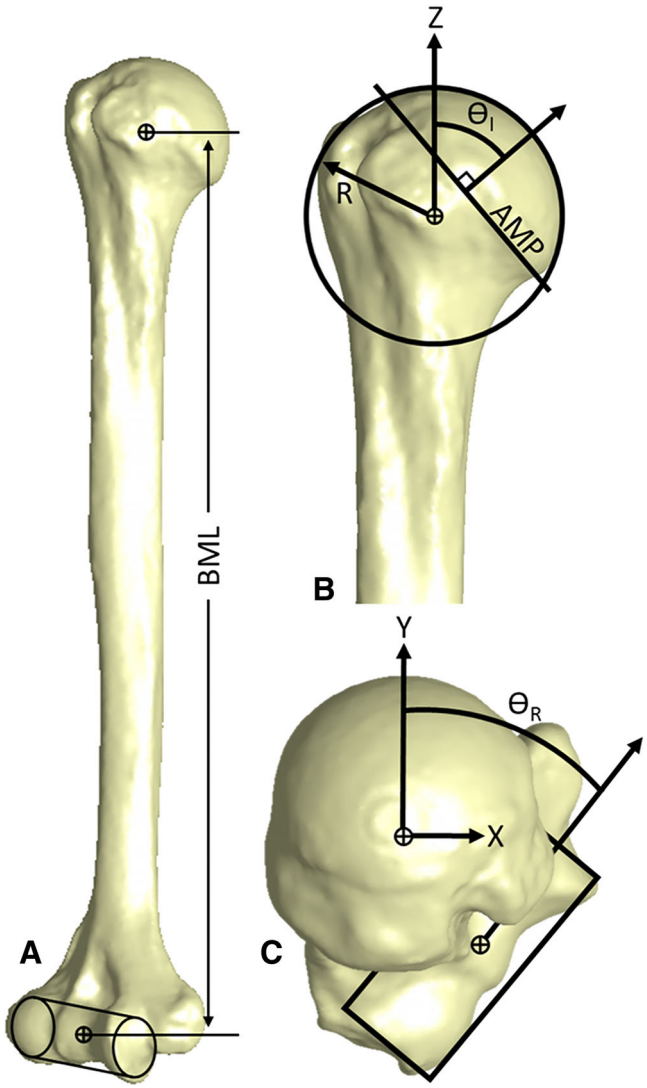

Fig. 2. (**A**) Biomechanical length (BML) was defined as the Z distance between humeral head center and center of the cylindrical axis of the elbow. (**B**) Inclination (θl) and head radius (R), (**C**) Retroversion (θR). Rigid body transformation of all surface reconstructions was applied to align the anatomic coordinate system of each bone with the global coordinate system within Amira.

All statistical testing was performed using Stata 13 (StataCorp LP, College Station, TX). Significance was set at $P \leq 0.050$.

RESULTS

Repeatability and Accuracy

Comparison of user-generated surface reconstructions with the MicroCT reference revealed a mean (range) RMS error of 0.26 mm (0.25–0.29 mm) and 0.15 (0.14–0.17 mm) for the periosteal surface and medullary diaphysis, respectively. RMS error was below voxel resolution and reveals that improved segmentation accuracy was achieved in the diaphyseal region of the bone where periosteal and endosteal cortical boundaries are more defined. Interoperator repeatability of anatomic landmark selection and calculation of external morphologic measures showed excellent agreement, defined as the lower bound of the 95% confidence interval on the ICC exceeding 0.9 (Koo and Li, 2016). Lower bound ICC values for head radius, inclination, retroversion, and BML and were 0.992, 0.923, 0.986, and 0.999, respectively.

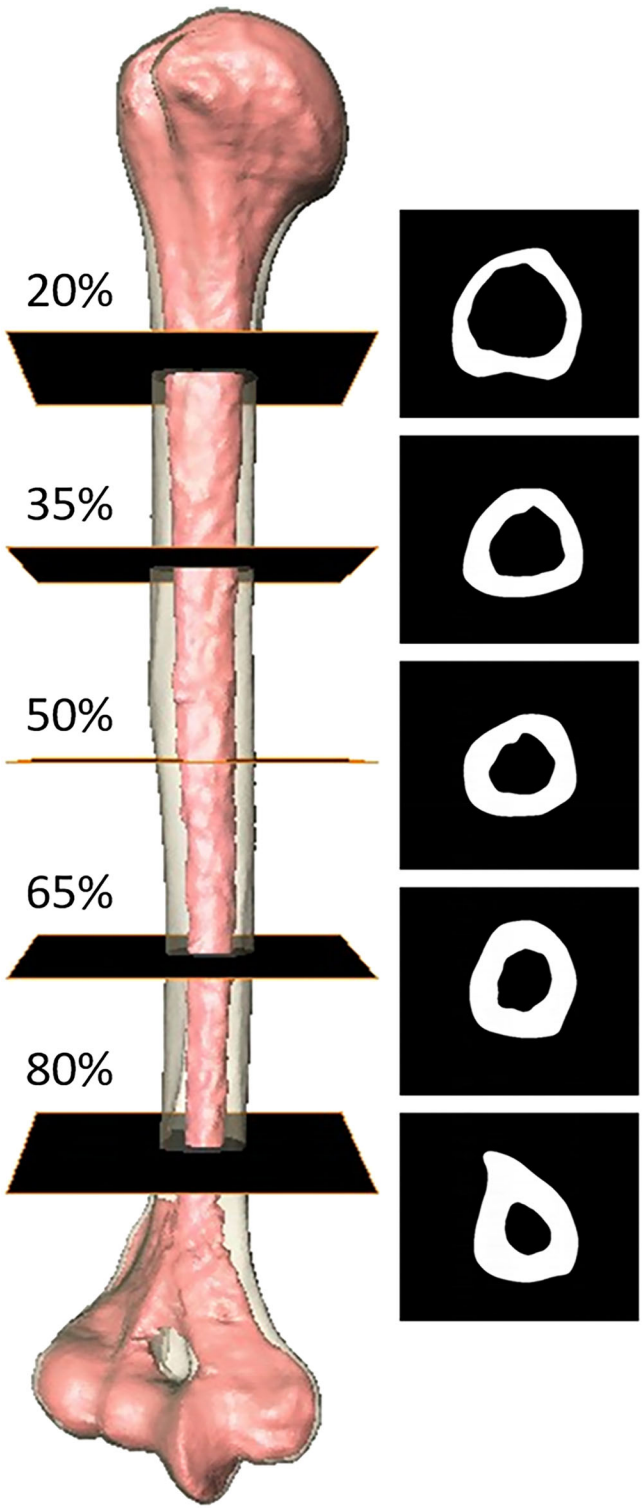

Fig. 3. Surface reconstruction of a right humerus displaying cross-sections at 20, 35, 50, 65, and 80% of BML.

Humeral Length, Head Radius, Inclination, and Retroversion

Right specimens exhibited greater BML and retroversion than left (Table 1, $P = 0.022$ and $P \leq 0.001$, respectively). No laterality differences were observed in humeral head radius or inclination. Males displayed greater BML and humeral head radius than females ($P \leq 0.001$). No sex differences were observed in inclination or retroversion.

Medullary Orientation

Distal diaphyseal retroversion is similar in magnitude to that measured at the cylindrical axis of the condyles. The principal orientation proceeds proximally in anteversion until a conformational change in principal orientation occurs at approximately 65% BML and shifts the principal orientation back into retroversion. This trend in retroversion continues for the remainder of the humeral diaphysis. At 20% BML, the canal exhibits retroversion for all groups (male, female, right, and left) with female subjects exhibiting significantly higher retroversion proximally than males (Fig. 4, $*P = 0.001$).

1st, 2nd Principal Diameter, and Aspect Ratio

Significantly larger 1st and 2nd principal medullary diameters were observed in right humeri at all analyzed locations (20, 35, 50, 65, 80% BML) with the exception of 80% BML in the 1st principal direction (Fig. 5, $*P \leq 0.024$). No difference in aspect ratio was observed between left and right humeri. Males exhibited significantly larger diameters in the proximal humerus (Fig. 6, $*P \leq 0.017$) with overlap in medullary diameters distally. Females exhibited significantly higher medullary aspect ratio at the 35 and 50% BML levels (Fig. 6, $*P \leq 0.014$).

Mean Cortical Thickness

Laterality differences in mean cortical thickness showed that the left humerus exhibited greater cortical thickness at the proximal diaphysis (Fig. 7, 20% BML, $*P = 0.048$). Differences between males and females showed males possess significantly higher cortical thickness at all evaluated levels ($*P \leq 0.001$). All groups exhibited decreased cortical thickness proximally with values approaching a plateau in the distal 50% of the diaphysis.

Medullary Taper

Male specimens exhibited a substantial increase in the rate of medullary expansion from distal to proximal with a break point located near 50% BML in both the 1st and 2nd principal directions (Table 2). Females exhibited a similar increase in the 2nd principal direction with a break point located at 58% BML. No break point in females was observed along the 1st principal direction, as the rate of medullary expansion remained constant over the length of the diaphysis.

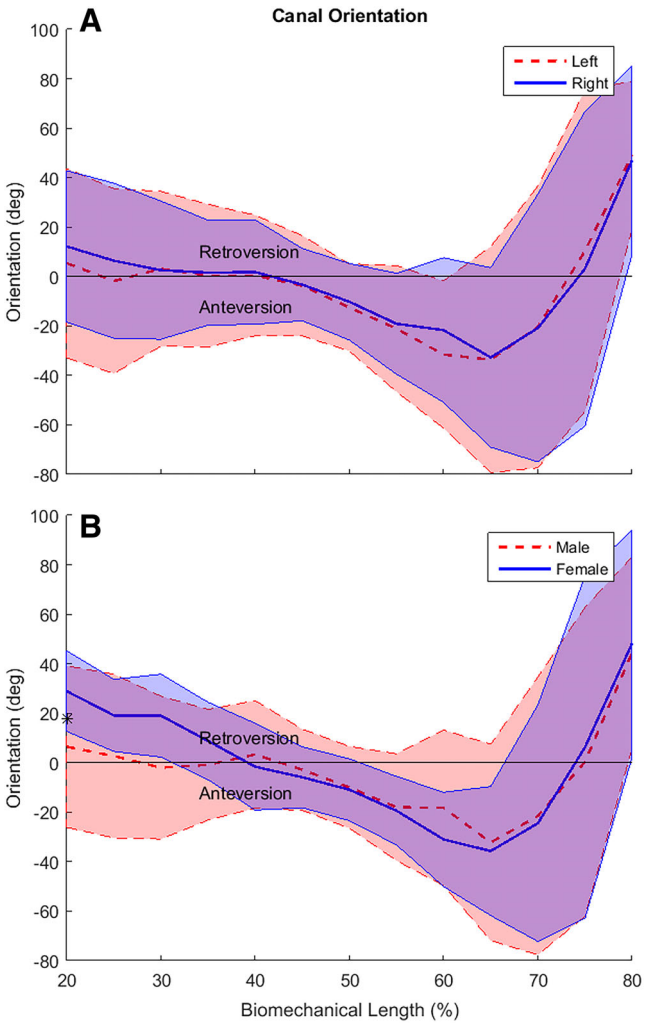

Fig. 4. Canal orientation plotted as a function of BML. Bold solid or dashed line and corresponding shaded region represent mean and ± 1 standard deviation. (**A**) Male (red --)/Female (blue –), (**B**) Right (red --)/Left (blue –). *Denotes statistically significant difference, $P = 0.001$.

Stratification by Age

In female humeri, there were 5 specimens aged 21–40 (median 32 years) and 10 aged 41–66 (median 57 years).

TABLE 1. Summary of external morphology results

	Mean (SD)			Mean (SD)		
Measure	Left	Right	*P* value	Male	Female	*P* value
BML (mm)	291.4 (20.6)	292.2 (23.7)	0.022	298.3 (24.5)	274.6 (21.1)	≤0.001
Head radius (mm)	23.6 (2.0)	23.7 (2.1)	0.253	24.5 (1.5)	21.1 (1.0)	≤0.001
Inclination (degree)	130.1 (4.3)	130.4 (3.7)	0.556	130.6 (3.6)	129.8 (4.1)	0.470
Retroversion (degree)	36.0 (10.2)	42.2 (10.5)	≤0.001	42.4 (10.6)	41.8 (10.6)	0.836

Four anatomic characteristics examined in 58 paired humeri (43 males, 15 females).

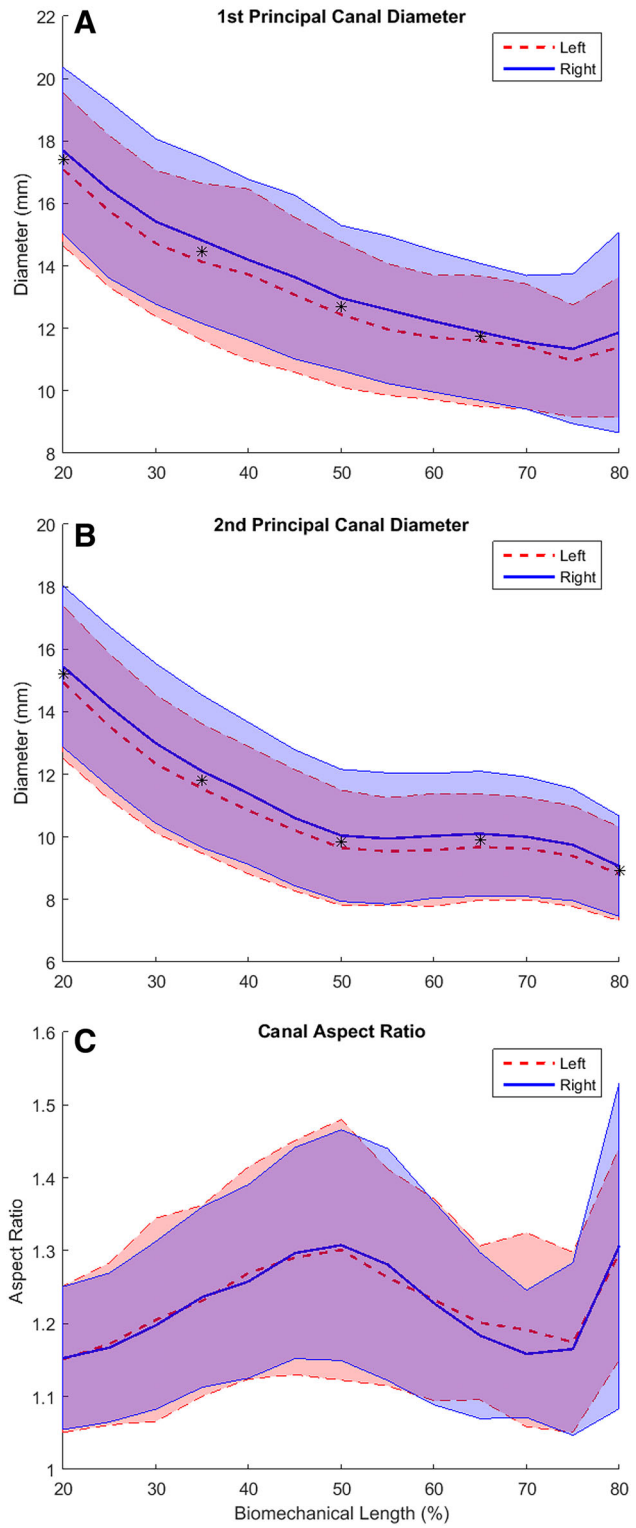

Fig. 5. (**A**) 1st and (**B**) 2nd principal canal diameters and (**C**) canal aspect ratio as a function of BML. *Denotes statistically significant difference, $P \leq 0.024$.

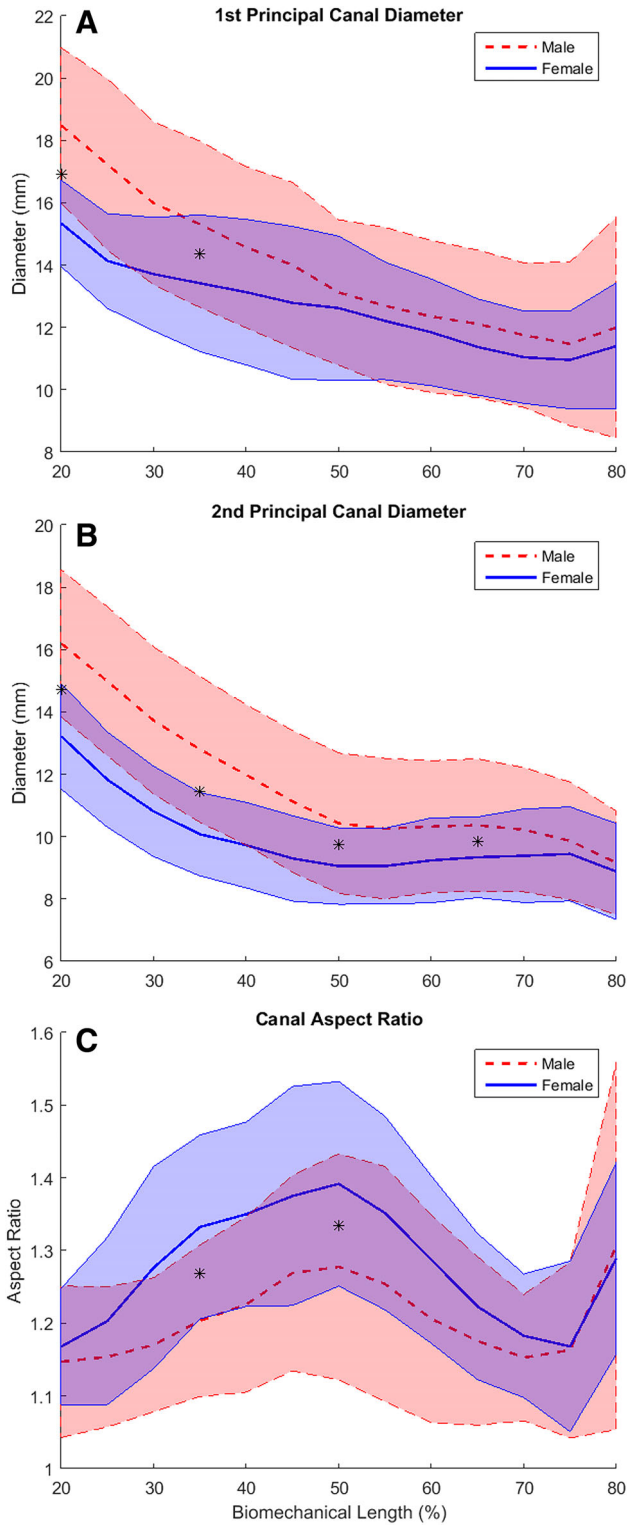

Fig. 6. (**A**) 1st and (**B**) 2nd principal canal diameters and (**C**) canal aspect ratio as a function of BML. *Denotes statistically significant difference, $P \leq 0.017$.

No significant differences were detected in these age groups for any of the measurements. Applying the same 40-year age cutoff to the male humeri yielded 12 specimens aged 18–40 (median 27 years) and 31 aged 41–74 (median 56 years). In this case, statistically significant age-related changes in the proximal diaphysis are observed with 10% reduction in

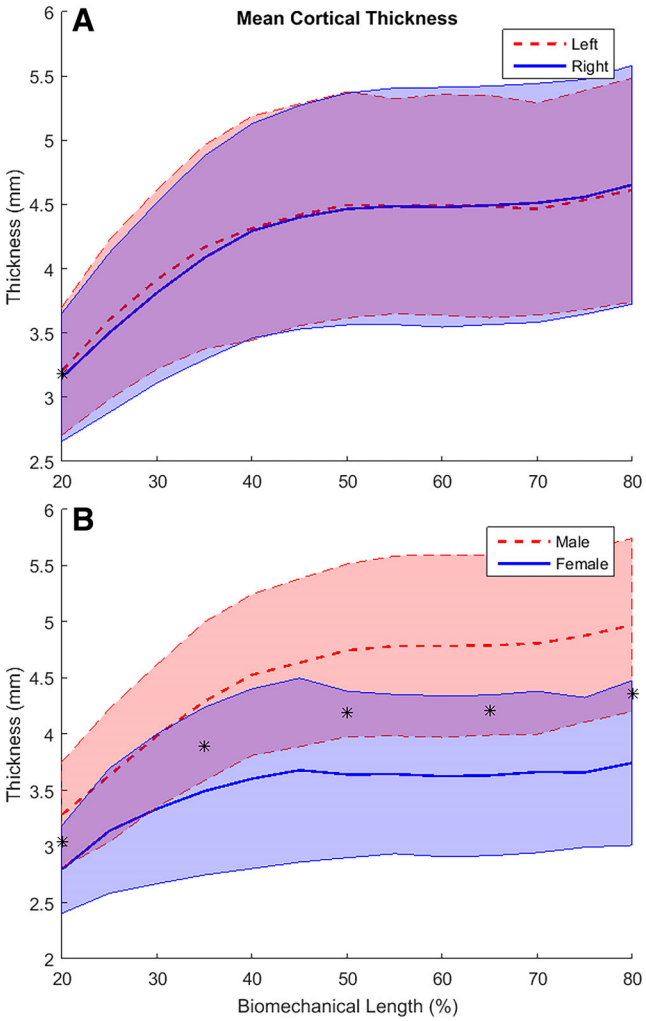

Fig. 7. Cortical thickness as a function of BML. (**A**) Right/Left, (**B**) Male/Female. *Denotes statistically significant difference, $P \leq 0.048$.

mean cortical thickness at the proximal (20% BML) level ($P < 0.028$). Additionally, endosteal expansion along the 2nd principal diameter was observed at the 20, 35, 50, and 65% BML levels with an average medullary diameter increase of 15% ($P \leq 0.040$).

DISCUSSION

The goal of OI prosthetic fixation is to improve the daily function of those suffering from an amputation by removing the barriers to prosthetic use often encountered in traditional socket suspension. To achieve this goal in patients with transhumeral amputation, it is important for engineers, surgeons, and prosthetists to understand the medullary and periosteal morphology of the humerus. Understanding of medullary morphology affects endoprosthetic design, sizing, and fixation strategies while the relationship to periosteal morphology holds implications for prosthetic fitting and the kinematic loading environment of the implant. These design cues are not limited to OI implants, but can also inform the design of other systems seeking diaphyseal placement in the humerus, such as megaprostheses for trauma and cancer reconstruction where component loosening is a common complication (Kulkarni et al., 2003; Hanna et al., 2007; Funovics et al., 2011).

This study demonstrated that the use of nondestructive, three-dimensional techniques produces accurate bony surface reconstructions with RMS errors at or below voxel resolution for the periosteal and medullary endosteal surfaces. A reproducible anatomic coordinate system was also constructed from proximal bony features for evaluation of both periosteal and medullary morphology. This anatomic coordinate system definition will allow translation of methods described here to amputee populations and those suffering traumatic disruption of the distal humerus or elbow.

Perhaps the greatest challenge to OI endoprosthetic placement within the medullary canal of the humerus comes from the diverging nature of the medullary space. Unlike total joint applications, where the metaphyseal flare of long bones lends itself to press-fit stem insertion, the geometric constraints of implant insertion and the diverging medullary space limits the ability to obtain apposition of bone ingrowth surfaces with endosteal bone without extensive preparation (reaming/broaching) of the cortex that may result in thin cortical walls that increase fracture risk under complex upper extremity loading (Drew et al., 2017). This challenge is amplified in the proximal medullary canal, beyond the calculated break point, where among male specimens, the rate of medullary divergence increases three and seven times in the 1st and 2nd principal directions, respectively (Table 2). In female specimens, the rate of medullary expansion remains constant in the 1st principal direction and transitions from parallel to divergent in the 2nd principal direction. Simultaneously, the mean cortical thickness diminishes precipitously in the proximal cortex (Fig. 7). As a result, proximal stem fixation may

TABLE 2. Canal taper as a function of total BML for males and females

Measure	Direction	Coefficient		*P* value
		Male	Female	
Distal taper (mm/100% BML)	1st principal diameter	5.3	6.8[a]	0.094
	2nd principal diameter	2.8	−0.5	0.001
Break point (% BML)	1st principal diameter	49	N/A[a]	N/A
	2nd principal diameter	54	58	N/A
Proximal taper (mm/100% BML)	1st principal diameter	16.6	6.8[a]	0.001
	2nd principal diameter	19.8	15.9	0.009

[a]Linear fit substituted for piecewise linear fit resulting in a single slope value and no break point.

need to be achieved through methods not relying solely on press-fit stabilization for ingrowth (Farfalli et al., 2009).

Despite the increasing rate of medullary canal expansion from the distal to proximal diaphysis, only small differences were observed in the diameter of the distal medullary space between men and women (Fig. 6). However, while overall size variation is limited, females do exhibit significantly thinner cortical bone at all levels (Fig. 7), and an increased aspect ratio of the medullary space (Fig. 6). This decline in cortical bone and circularity may pose a challenge for implants that possess a circular cross-section, as an inherent mismatch is cross-sectional geometry may necessitate more bone removal than an anatomic or asymmetric endoprosthesis.

The use of noncircular implant geometries faces another challenge in the continuous rotational axial component of humerus morphology first described by Descamps et al. (2009). Of particular interest to endoprosthetic apposition is the conformational switch in medullary orientation that is exhibited near 35% BML (Fig. 4). This is analogous to squeezing an ellipse along its major axis until a 90-degree shift in the orientation of the major axis occurs. Placement of an endoprosthesis at this level may inherently result in a rotational shift in the location of bony apposition as the orientation indicates the direction of largest medullary diameter.

The periosteal measure of retroversion supports previous studies that have reported increased humeral retroversion on the dominant side (Kronberg et al., 1990; Cassagnaud et al., 2003; Table 1). The magnitude in mean difference between left and right humeri, 6.2 degrees, was less than 7.9 degrees reported by DeLude et al.; however, in that study higher values of retroversion were noted for the left side (DeLude et al., 2007). The magnitude of retroversion measures were also similar to those reported by Delude et al. and similarities can be attributed to the comparable anatomic coordinate system definitions (DeLude et al., 2007). While the clinical significance for OI prosthetic fixation is not well understood at this time, variation in retroversion may carry implications for elbow axis alignment during prosthetic fitting. No differences were observed in humeral head inclination between groups (Table 1).

Males displayed increased BML when compared to females (Table 1). This result indicates that for a comparable amputation level, and re-creation of intact anatomy, the bone-implant interface in male subjects will experience higher loads due to the increased moment arm distal to the amputation (Drew et al., 2017). Despite this increased load, stresses and fracture risk may remain higher in the female population due to the decreased amount of cortical bone present. This dependence of loading on humeral length, and amputation level, supports the need for overload protection devices to maximize return to function without compromising implant fixation in this unique population (Jonsson et al., 2011).

Stratification by age yielded mixed results between female and male humeri, but this was expected as the study was not specifically powered by adequate sample sizes within each gender. This was in part due to practical limitations in obtaining cadaver specimens with sufficient diversity to examine subgroups by age. While there were some differences in cortical thickness, endosteal expansion, and medullary diameter in males, the female cohort was too small to detect changes. Based on the trends in the female data, an increased sample size in future studies might also detect a reduction in cortical thickness and a corresponding increase in medullary diameter.

This study is subject to limitations. First, humeri were collected from a normal cadaver population. Application of morphologic results to the amputee population may not be appropriate for all measures as trauma and cortical remodeling due to the modified loading environment can alter normal anatomy (Dequeker, 1971; Lang et al., 2006; McCarthy et al., 2012). Grouping of humeri by hand dominance instead of laterality may impact the statistical relationships and would be more appropriate if data were available in donor summaries (Crockett et al., 2002; Reagan et al., 2002). Additionally, the limited number of female subjects may have resulted in under-sampling of the range of variability present in the female population.

CONCLUSION

Three-dimensional measurement of medullary and periosteal morphology from CT images was an accurate and effective quantification method. Our findings establish the most comprehensive analysis of medullary morphology in the humerus to date and expand the current body of literature on periosteal morphology of the humerus. This information is important to the design of OI implant systems for upper extremity amputees, and can find application in megaprostheses, and in traditional shoulder and elbow arthroplasty. This study also establishes a framework for future studies examining structural remodeling of the humerus following amputation.

ACKNOWLEDGMENTS

This work was supported in part by the US Army Medical Research and Materiel Command under contract #W81XWH-15-C-0058, by the United States Department of Veterans Affairs Rehabilitation Research and Development Service under Merit Review Award #I01RX001246, and by the Department of Orthopaedics, University of Utah School of Medicine, Salt Lake City, Utah. The views, opinions, and/or findings presented are those of the authors and should not be construed as an official position, policy or decision of any of these funding sources unless so designated by other documentation. In the conduct of research where humans are the subjects, the investigator(s) adhered to the policies regarding the protection of human subjects as prescribed by Code of Federal Regulations (CFR) Title 45, Volume 1, Part 46; Title 32, Chapter 1, Part 219; and Title 21, Chapter 1, Part 50 (Protection of Human Subjects).

Literature Cited

Al Muderis M, Khemka A, Lord SJ, Van de Meent H, Frölke JPM. 2016. Safety of osseointegrated implants for transfemoral amputees: A two-center prospective cohort study. J Bone Joint Surgery Am 98:900–909.

Berke GM, Fergason J, Milani JR, Hattingh J, McDowell M, Nguyen V, Reiber GE. 2010. Comparison of satisfaction with current prosthetic care in veterans and servicemembers from Vietnam and OIF/OEF conflicts with major traumatic limb loss. J Rehabil Res Dev 47:361–371.

Biddiss E, Beaton D, Chau T. 2007. Consumer design priorities for upper limb prosthetics. Disabil Rehabil Assist Technol 2:346–357.

Biddiss E, Chau T. 2007a. Upper-limb prosthetics: Critical factors in device abandonment. Am J Phy Med Rehabil/Assoc Acad Physiat 86: 977–987.

Biddiss EA, Chau TT. 2007b. Upper limb prosthesis use and abandonment: A survey of the last 25 years. Prosthet Orthot Int 31: 236–257.

Brownhill JR, King GJ, Johnson JA. 2007. Morphologic analysis of the distal humerus with special interest in elbow implant sizing and alignment. J Shoulder Elbow Surg 16:S126–S132.

Cassagnaud X, Maynou C, Petroff E, Dujardin C, Mestdagh H. 2003. A study of reproducibility of an original method of CT measurement of the lateralization of the intertubercular groove and humeral retroversion. Surg Radiol Anat 25:145–151.

Crockett HC, Gross LB, Wilk KE, Schwartz ML, Reed J, O'Mara J, Reilly MT, Dugas JR, Meister K, Lyman S, et al. 2002. Osseous adaptation and range of motion at the glenohumeral joint in professional baseball pitchers. Am J Sports Med 30:20–26.

DeLude JA, Bicknell RT, MacKenzie GA, Ferreira LM, Dunning CE, King GJ, Johnson JA, Drosdowech DS. 2007. An anthropometric study of the bilateral anatomy of the humerus. J Shoulder Elbow Surg 16: 477–483.

Dequeker J. 1971. Periosteal and endosteal surface remodeling in pathologic conditions. Invest Radiol 6:260–265.

Descamps S, Moreel P, Garcier JM, Bouillet B, Brehant J, Tanguy A. 2009. Existence of a rotational axial component in the human humeral medullary canal. Surgical and radiologic anatomy : SRA 31:579–583.

Drew AJ, Izykowski MT, Bachus KN, Henninger HB, Foreman KB. 2017. Transhumeral loading during advanced upper extremity activities of daily living. PLoS One 12:e0189418.

Engh CA, O'Connor D, Jasty M, McGovern TF, Bobyn JD, Harris WH. 1992. Quantification of implant micromotion, strain shielding, and bone resorption with porous-coated anatomic medullary locking femoral prostheses. Clin Orthop Relat Res (285):13–29.

Farfalli GL, Boland PJ, Morris CD, Athanasian EA, Healey JH. 2009. Early equivalence of uncemented press-fit and compress femoral fixation. Clin Orthop Relat Res 467:2792–2799.

Funovics PT, Schuh R, Adams SB Jr, Sabeti-Aschraf M, Dominkus M, Kotz RI. 2011. Modular prosthetic reconstruction of major bone defects of the distal end of the humerus. J Bone Joint Surg Am 93:1064–1074.

Gebhart JJ, Miniaci A, Fening SD. 2013. Predictive anthropometric measurements for humeral head curvature. J Shoulder Elbow Surg 22:842–847.

Goldberg SH, Omid R, Nassr AN, Beck R, Cohen MS. 2007. Osseous anatomy of the distal humerus and proximal ulna: Implications for total elbow arthroplasty. J Shoulder Elbow Surg 16:S39–S46.

Hagberg K, Branemark R. 2009. One hundred patients treated with osseointegrated transfemoral amputation prostheses--rehabilitation perspective. J Rehabil Res Dev 46:331–344.

Hanna SA, David LA, Aston WJ, Gikas PD, Blunn GW, Cannon SR, Briggs TW. 2007. Endoprosthetic replacement of the distal humerus following resection of bone tumours. J Bone Joint Surg Br 89:1498–1503.

Jeyapalina S, Beck JP, Bloebaum RD, Bachus KN. 2014. Progression of bone ingrowth and attachment strength for stability of percutaneous osseointegrated prostheses. Clin Orthop Relat Res 472:2957–2965.

Johnson JW, Thostenson JD, Suva LJ, Hasan SA. 2013. Relationship of bicipital groove rotation with humeral head retroversion: A three-dimensional computed tomographic analysis. J Bone Joint Surg Am 95:719–724.

Jones RH, Molitoris BA. 1984. A statistical method for determining the breakpoint of two lines. Anal Biochem 141:287–290.

Jonsson S, Caine-Winterberger K, Branemark R. 2011. Osseointegration amputation prostheses on the upper limbs: Methods, prosthetics and rehabilitation. Prosthet Orthot Int 35:190–200.

Juhnke DL, Beck JP, Jeyapalina S, Aschoff HH. 2015. Fifteen years of experience with integral-leg-prosthesis: Cohort study of artificial limb attachment system. J Rehabil Res Dev 52:407–420.

Kang NV, Pendegrass C, Marks L, Blunn G. 2010. Osseocutaneous integration of an intraosseous transcutaneous amputation prosthesis implant used for reconstruction of a transhumeral amputee: Case report. J Hand Surg Am 35:1130–1134.

Kapron AL, Aoki SK, Peters CL, Maas SA, Bey MJ, Zauel R, Anderson AE. 2014. Accuracy and feasibility of dual fluoroscopy and model-based tracking to quantify in vivo hip kinematics during clinical exams. J Appl Biomech 30:461–470.

Koo TK, Li MY. 2016. A guideline of selecting and reporting intraclass correlation coefficients for reliability research. J Chiropr Med 15:155–163.

Kronberg M, Brostrom LA, Soderlund V. 1990. Retroversion of the humeral head in the normal shoulder and its relationship to the normal range of motion. Clin Orthop Relat Res (253):113–117.

Kulkarni A, Fiorenza F, Grimer RJ, Carter SR, Tillman RM. 2003. The results of endoprosthetic replacement for tumours of the distal humerus. J Bone Joint Surg Br 85:240–243.

Lang TF, Leblanc AD, Evans HJ, Lu Y. 2006. Adaptation of the proximal femur to skeletal reloading after long-duration spaceflight. J Bone Miner Res 21:1224–1230.

McCarthy ID, Bloomer Z, Gall A, Keen R, Ferguson-Pell M. 2012. Changes in the structural and material properties of the tibia in patients with spinal cord injury. Spinal Cord 50:333–337.

Pearl ML, Volk AG. 1996. Coronal plane geometry of the proximal humerus relevant to prosthetic arthroplasty. J Shoulder Elbow Surg 5: 320–326.

Reagan KM, Meister K, Horodyski MB, Werner DW, Carruthers C, Wilk K. 2002. Humeral retroversion and its relationship to glenohumeral rotation in the shoulder of college baseball players. Am J Sports Med 30:354–360.

Robertson DD, Yuan J, Bigliani LU, Flatow EL, Yamaguchi K. 2000. Three-dimensional analysis of the proximal part of the humerus: Relevance to arthroplasty. J Bone Joint Surg Am 82-A:1594–1602.

Shelton TJ, Beck JP, Bloebaum RD, Bachus KN. 2011. Percutaneous osseointegrated prostheses for amputees: Limb compensation in a 12-month ovine model. J Biomech 44:2601–2606.